Journal Name

ARTICLE

Enhancing thermostability of iron ethylene polymerization catalysts through *N,N,N*-chelation of doubly fused α,α′-bis(arylimino)-2,3:5,6-bis(hexamethylene)pyridines

Received 00th xx 20xx,
Accepted 00th xx 20xx

DOI: 10.1039/x0xx00000x

www.rsc.org/

Zheng Wang,[a,b] Randi Zhang,[a,b] Wenjuan Zhang,*[,c] Gregory A. Solan,*[,a,d] Qingbin Liu,*[,e,] Tongling Liang[a,b] and Wen-Hua Sun*[,a,b,]

The ferrous chloride complexes, [2,3:5,6-{$C_5H_{10}C(NAr)$}$_2C_5HN$]$FeCl_2$ (Ar = 2,6-Me_2Ph **Fe1**, 2,6-Et_2Ph **Fe2**, 2,6-i-Pr_2Ph **Fe3**, 2,4,6-Me_3Ph **Fe4**, 2,6-Et_2-4-MePh **Fe5**), each bearing a *N,N,N*-ligand incorporating two partially saturated fused eight-membered rings, have been synthesized by the one-pot template reaction of α,α'-dioxo-2,3:5,6-bis(hexamethylene)pyridine, iron(II) chloride tetrahydrate and the corresponding aniline in acetic acid. The structures of **Fe3** and its oxidized diferric derivative, [2,3:5,6-{$C_5H_{10}C(N(2,6\text{-i-}Pr_2Ph))$}$_2C_5HN$]$FeCl(\mu\text{-}O)FeCl_3$ (**Fe3'**), revealed square pyramidal geometries with either a chloride or an oxo ligand filling the apical sites, respectively. On treatment with either methylaluminoxane (MAO) or modified methylaluminoxane (MMAO), all precatalysts displayed good thermostability (optimal operating temperatures: 50 – 80 °C) and moreover delivered exceptionally high activities for ethylene polymerization [up to 12.23×10^6 g(PE) mol^{-1} (Fe) h^{-1}] producing highly linear polyethylene of high molecular weight (M_w up to 62.5 kg mol^{-1} even at 80 °C). The catalytic activities fall in the order, **Fe1** > **Fe4** > **Fe2** > **Fe5** > **Fe3** (MMAO or MAO), with both steric and electronic factors influential; iron(III)-containing **Fe3'** was less active. Distinct chain termination processes for the polymerizations have been identified through end-group analysis with both β-H elimination and chain transfer to aluminum operative with MMAO, while only transfer to aluminum has been detectable with MAO. Notably with MMAO, the different rates of these termination processes manifests itself in bimodal molecular weight distributions for the polyethylenes.

Introduction

Over twenty years ago Brookhart[1] and Gibson[2] independently reported that activation of 2,6-bis(arylimino)pyridine-iron(II) and -cobalt(II) halide complexes with methylaluminoxane (MAO) afford effective catalysts for the conversion of ethylene into either high density polyethylene (HDPE) or into α-olefins with Schulz–Flory distributions.[3] In the intervening years a host of different skeletal modifications have been made to the bis(imino)pyridine framework (**A**, Chart 1),[3,4] culminating in improvements to both catalytic activity and thermostability.[4] Elsewhere, alternative pyridine-based ligand sets have emerged as compatible supporting frameworks for active iron and cobalt oligo-/polymerization catalysis;[3c-e] some notable examples include 2-imino-1,10-phenanthrolines,[5] 2-benzimidazolyl-6-iminopyridines,[6] *N*-[(pyridin-2-yl)methylene]-8-aminoquinolines[7] and 2,8-bis(imino)quinolines.[8,3c-e] From an industrial standpoint, the integration of a 2-imino-1,10-phenanthroline-iron catalyst into a 500-ton scale pilot process for ethylene oligomerization highlights the potential of this technology.[3e,5c] However, the susceptibility of the parent bis(imino)pyridine-iron family of polymerization catalysts towards deactivation at higher operating temperatures has, in some measure, impeded further industrial developments. In particular, pathways involving alkylation reactions of the ligand frame or deprotonation chemistry involving the imino-C methyl groups have been proposed as likely deactivation routes.[9,10] Nevertheless, some progress in addressing these deleterious side reactions has been made through the introduction of more inert substituents to the imino carbon atoms and indeed some improved thermal stability of the catalyst has been observed.[11]

In recent years, our group and others have found that the fusion of cycloalkyl units to the central pyridine in **A** (Chart 1) can be influential on the chelation properties of the ligand in the resultant iron or cobalt catalyst.[11-16] Furthermore, variations in ligand strain imparted by ring size changes have been shown to not not only impact on the activity of the catalyst but also on the

[a.] *Key Laboratory of Engineering Plastics and Beijing National Laboratory for Molecular Science, Institute of Chemistry, Chinese Academy of Sciences, Beijing 100190, China.*
[b.] *CAS Research/Education Center for Excellence in Molecular Sciences, University of Chinese Academy of Sciences, Beijing 100049, China.*
[c.] *Beijing Key Laboratory of Clothing Materials R&D and Assessment, Beijing Engineering Research Center of Textile Nanofiber, School of materials Science and Engineering, Beijing institute of Fashion Technology, Beijing 100029, China.*
[d.] *Department of Chemistry, University of Leicester, University Road, Leicester LE1 7RH, UK.*
[e.] *College of Chemistry and Material Science, Hebei Normal University, Shijiazhuang 050024, China.*
**Corresponding Authors: zhangwj@bift.edu.cn (W.Z.); liuqingb@sina.com (Q.L.); gas8@leicester.ac.uk (G.A.S.); whsun@iccas.ac.cn, Tel: +86-10-62557955; Fax: +86-10-62618239 (W.-H.S).*

Electronic Supplementary Information (ESI) available: Figures, Tables S1 - S6, and DSC thermograms of the polyethylenes and X-ray crystallographic data in CIF for CCDC 1887902 (**Fe3**) and 1887903 (**Fe3'**) available free of charge from the Cambridge Crystallographic Data Centre. See DOI: 10.1039/x0xx00000x

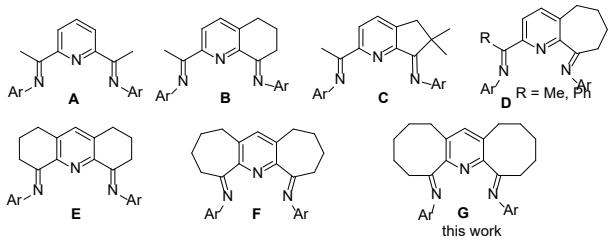

Chart 1 Ligand frameworks **B** - **G** derived from bis(imino)pyridine **A**

properties of the resulting polymeric material.[3c-e,11-16] With regard to the ligand set, both singly fused examples such as **B**,[12] **C**[13] and **D**[11,14] (Chart 1) incorporating six, five and seven-membered rings, respectively, as well as doubly fused **E**[15] and **F**[16] (Chart 1) containing six and seven-membered rings, are all synthetically accessible. In terms of catalytic performance, iron complexes bearing **B**,[12a] **D**[11a,14a] and **F**[16a] are capable of polymerizing ethylene with high activities in the order of 10^7 g (PE) mol^{-1}(Fe) h^{-1} generating strictly linear polyethylenes with a range of molecular weights and end-group types.[16a] By contrast, iron precatalysts based on the **E**-type ligand produced mixtures of both polyethylenes and oligomers.[15]

In this work we are concerned with the fusion of two eight membered rings to the central pyridine in **A** to form α,α'-bis (arylimino)-2,3:5,6-bis(hexamethylene)pyridine **G** (Chart 1) and the effect this structural variation has on the catalytic performance and thermal stability of the resulting iron catalyst. It is envisaged that these larger rings will lead to reduced ligand strain in a manner similar to that observed with cyclophane-type ligands,[17] while presenting a well-defined and sterically protected cavity for the polymerization to occur. Indeed, the compatibility of **G** as a support for highly active cobalt catalysts has recently been disclosed.[18] Herein we report the synthesis of five examples of ferrous chloride complexes containing **G** that differ in the steric and electronic properties of the N-aryl groups. An in-depth catalytic evaluation using two different aluminoxane activators is then conducted to ascertain how these precatalyst and co-catalyst variations impact on the polymer product, catalytic activity and thermo-stability; the effect of precatalyst oxidation state on performance is a further point of interest. In addition to the polymer characterization, full synthetic and characterization details are presented for all iron complexes.

Results and Discussion

Synthesis and Characterization of the iron precatalysts

The iron(II) complexes, [2,3:5,6-{$C_5H_{10}C(NAr)$}$_2C_5HN$]$FeCl_2$ (Ar = 2,6-Me_2Ph **Fe1**, 2,6-Et_2Ph **Fe2**, 2,6-i-Pr_2Ph **Fe3**, 2,4,6-Me_3Ph **Fe4**, 2,6-Et_2-4-MePh **Fe5**), have each been prepared by the template reaction of α,α'-dioxo-2,3:5,6-bis(hexamethylene)pyridine,[18] iron(II) chloride tetrahydrate and two equivalents of the corresponding aniline in acetic acid at reflux; similar one-pot approaches have been employed for a range of related iron[14a,15,16a] and cobalt compounds.[14b,16b,18] Following work-up, **Fe1 - Fe5** were isolated as blue solids in good yields that proved stable in the solid state but underwent oxidation on prolonged standing in solution (Scheme 1). To explore the nature of the oxidized product, a dichloromethane solution of **Fe3** was additionally stirred at room temperature under an oxygen atmosphere (or 120 hours under air) affording the diferric species [2,3:5,6-{$C_5H_{10}C(N(2,6\text{-i-}Pr_2Ph))$}$_2C_5HN$]$FeCl(\mu\text{-}O)FeCl_3$ (**Fe3'**) as a yellow solid in good yield.[19] All iron complexes have been characterized by FT-IR spectroscopy elemental analysis and in the case of **Fe3** and **Fe3'** by single crystal X-ray diffraction.

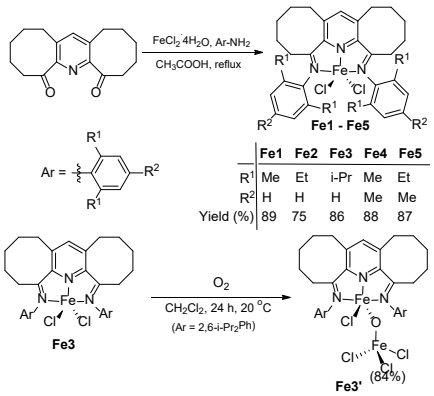

Scheme 1 Synthetic routes to **Fe1** – **Fe5** and **Fe3'**

Crystals of **Fe3** suitable for the X-ray determination were grown under a nitrogen atmosphere by slow diffusion of hexane into a tetrahydrofuran solution of the complex maintained at room temperature. On the other hand, crystals of **Fe3'** were obtained by layering a dichloromethane solution of the complex with diethyl ether in the presence of air. **Fe3** crystallized as two independent molecules (*A* and *B*) in the unit cell that are essentially the same that differ only in the positioning of the $FeCl_2$ unit within the *N,N,N* cavity. Views of **Fe3** (*molecule A*) and **Fe3'** are shown in Figures 1 and 2; selected bond distances and angles are presented for both in Table 1. The structures show some key differences and hence will be discussed separately while discussion of bond parameters for **Fe3** will be concerned with solely *molecule A*.

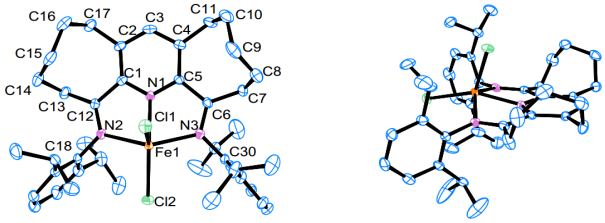

Figure 1 ORTEP representations of **Fe3** (*molecule A*). Thermal ellipsoids are shown at the 30% probability level while the hydrogen atoms have been omitted for clarity.

Fe3 comprises a single iron center surrounded by three nitrogen atoms belonging to the tridentate ligand (N1, N2 and N3) and two chlorides (Cl1 and Cl2) to complete a penta-coordinate geometry. This geometry can be best described as distorted square pyramidal with the three nitrogen atoms and Cl1 forming the base and Cl2 the apical position; the iron atom lies at a distance of 0.596 Å above the basal plane, which is slightly longer than that seen in its iron counterparts bearing **A** (0.09 - 0.56 Å),[2b,4a,4b] **B** (0.583 Å)[12a] and **D** [0.442 Å (R = Me[14a]) and 0.320 Å (R = Ph[11a])]. As is common to many bis(imino)pyridine-iron(II) complexes, the Fe–$N_{pyridyl}$ bond length [2.080(4) Å] is shorter than the exterior Fe–N_{imino} ones [2.157(4), 2.165(4) Å], which can be attributed to a combination of

the good donor properties of the central pyridine and the constraints of the ligand class.[12,14-16,18] Indeed, the Fe–$N_{pyridyl}$ bond length when compared with other iron(II) complexes including those bearing **A**,[1a,2b] **B**,[12a] **D**[11a,14a] and **F**[16a] (Chart 1) [range: 2.091(4) – 2.189(6) Å] is shorter but similar to that observed in **E** (2.087(4) Å).[15] Similarly, the Fe–N_{imino} bond distances in **Fe3** are shorter than those in iron-containing **A** [2.224(4) - 2.271(6) Å],[1a,2b] **B** [2.215(3) – 2.277(3) Å],[12a] **D** [2.210(8) – 2.255(7) Å],[11a,14a] **E** [2.313(4) – 2.320(4) Å][15] and **F** [2.261(2) – 2.272(2) Å],[16a] highlighting the good overall chelation properties of **G** to the iron center. The N-aryl rings in **Fe3** are almost perpendicular (84.70° and 84.33°) with respect to the neighboring imine unit in a manner that is similar to that seen in related (*N,N,N*)$FeCl_2$ complexes.[12,14-16,18] Furthermore, the N1–C5–C6–N3 and N1–C1–C12–N2 torsion angles are -2.31° and 11.36°, respectively, underlining the deviation from co-planarity between the pyridine ring and the neighboring imine vectors; a similar distortion has also been noted in its cobalt analogue.[18]

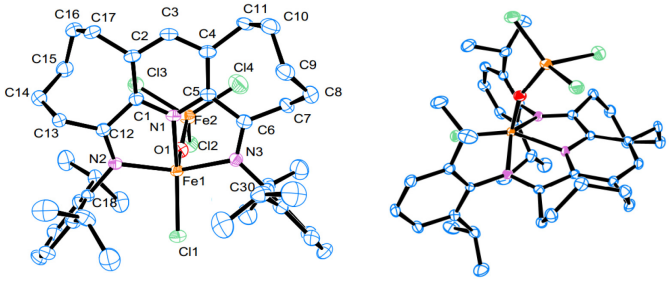

Figure 2 ORTEP representations of **Fe3'**. The thermal ellipsoids are shown at the 30% probability level and the hydrogen atoms have been omitted for clarity.

By contrast, the structure of **Fe3'** consists of a dinuclear core in which Fe1 and Fe2 are bridged by an oxo ligand. At Fe1 the nitrogen atoms of the chelating *N,N,N*-ligand and Cl1 form the basal plane of a square-based pyramidal geometry with O1 now the apical site, the iron atom is positioned 0.576 Å above the basal plane which is similar to that seen in (**A**)FeCl(μ-O)$FeCl_3$ (Ar = 2-i-Pr-6-MePh).[19a] On the other hand, at Fe2 three chloride ligands and the bridging oxo define the vertices of a distorted tetrahedron with the bond angles falling in the range 107.80(7) - 110.76(7)°. The Fe1-O1-Fe2 bond angle of 159.16(19)° comes in the mid-range for oxo-bridged diron(III) complexes.[19b] By comparison with **Fe3** and (**A**)FeCl(μ-O)$FeCl_3$[19a] (Ar = 2-i-Pr-6-MePh), only modest variations in the Fe1-N distances are apparent with the exterior distances marginally shorter {2.135(3), 2.149(3) Å (**Fe3'**) *vs.* [2.165(4), 2.157(4) Å (**Fe3**) and 2.197(7), 2.163(7) Å ((**A**)FeCl(μ-O)$FeCl_3$[19a])]} in **Fe3'** while the interior distance is longer [2.097(3) Å (**Fe3'**) *vs.* (2.080(4) Å (**Fe3**) and 2.076(7) Å ((**A**)FeCl(μ-O)$FeCl_3$[19a])]. Conversely, the Fe1-Cl distance in **Fe3'** (2.2131(12) Å) is markedly shorter than the Fe1-Cl distance in **Fe3** [2.3327(15), 2.2588(15) Å], which is likely due to the higher oxidation state of the metal center. Indeed, a similar observation was found in (**A**)FeCl(μ-O)$FeCl_3$.[19a] Once again, the N-aryl rings are inclined almost perpendicularly to the neighboring imine vectors (82.24° and 87.14°) while the N1–C5–C6–N3 (12.40°) and N1–C1–C12–N2 (-2.45°) reveal similar distortions than seen in **Fe3**. For both **Fe3** and **Fe3'**, the saturated sections of the two fused eight membered rings, C7-C8-C9-C10-C11 and C13-C14-C15-C16-C17, are puckered and both fold towards the apical chloride (**Fe3**) or oxo ligand (**Fe3'**), respectively.

Table 1 Selected bond lengths and angles for **Fe3** and **Fe3'**

Fe3			**Fe3'**	
	Bond lengths (Å)			
	Molecule A	*Molecule B*		
Fe1–N1	2.080(4)	2.086(4)	Fe1–N1	2.097(3)
Fe1–N2	2.165(4)	2.160(4)	Fe1–N2	2.135(3)
Fe1–N3	2.157(4)	2.174(4)	Fe1–N3	2.149(3)
Fe1–Cl1	2.3327(15)	2.3346(16)	Fe1–Cl1	2.2131(12)
Fe1–Cl2	2.2588(15)	2.2627(15)	Fe1–O1	1.776(3)
			Fe2-O1	1.764(3)
			Fe2-Cl2	2.2229(15)
			Fe2-Cl3	2.2048(14)
			Fe2-Cl4	2.2159(15)
	Bond angles (°)			
N1-Fe1-N2	74.05(16)	73.88(17)	N1-Fe1-N2	74.71(12)
N1-Fe1-N3	73.83(16)	74.11(16)	N1-Fe1-N3	73.68(13)
N1-Fe1-Cl1	87.87(12)	88.61(13)	N1-Fe1-Cl1	147.12(10)
N1-Fe1-Cl2	152.86(12)	150.89(13)	N2-Fe1-N3	141.84(12)
N2-Fe1-N3	139.70(17)	140.76(16)	N2-Fe1-Cl1	96.69(9)
N2-Fe1-Cl1	103.31(12)	100.44(12)	N2-Fe1-O1	103.83(13)
N2-Fe1-Cl2	96.70(12)	100.40(12)	O1-Fe1-N1	96.41(13)
N3-Fe1-Cl1	99.15(12)	100.90(12)	O1-Fe1-N3	100.43(13)
N3-Fe1-Cl2	100.90(13)	96.58(12)	O1-Fe1-Cl1	116.46(10)
Cl1-Fe1-Cl2	119.24(6)	120.43(6)	Fe1-O1-Fe2	159.16(19)
			Cl2-Fe2-Cl3	110.76(7)
			Cl2-Fe2-Cl4	107.80(7)
			Cl2-Fe2-O1	109.64(10)

The FT-IR spectra of **Fe1** – **Fe5** show C=N stretching frequencies that fall in the range 1591 – 1604 cm^{-1}, values that are quite typical of coordinated imine groups; no absorptions corresponding to coordinated C=O groups nor free diketone could be detected.[20] For **Fe3'** an absorption at 844 cm^{-1} can be assigned to an Fe-O-Fe asymmetric stretch as has been observed for a raft of related oxide-bridged iron(III) complexes.[19] Furthermore, the microanalytical data for the **Fe1** – **Fe5** and **Fe3'** are in agreement with the elemental compositions proposed.

Ethylene polymerization studies

With a view to exploring the capacity of **Fe1 - Fe5** and **Fe3'** to serve as precatalysts for ethylene polymerization, two different aluminoxanes, namely methylaluminoxane (MAO) and modified methylaluminoxane (MMAO), were screened as potential co-catalysts.[11-16] All resulting polymers have been characterized by gel permeation chromatography (GPC) and differential scanning calorimetry (DSC), while the microstructural properties of selected samples were examined using high temperature ^{13}C NMR spectroscopy. In all cases, gas chromatography was used to detect the presence of any oligomeric products.

(a) ***Catalytic evaluation using Fe1 – Fe5 and Fe3' with MMAO as co-catalyst.***

To establish the optimum conditions with MMAO as the co-catalyst, **Fe1** was selected as the test precatalyst for the polymerization. With the ethylene pressure maintained at 10 atm, the influence of the polymerization temperature, the aluminum to iron molar ratio (Al:Fe) and the run time have all been studied; the results of the catalytic evaluation are compiled in Table 2.

Firstly, the effect of temperature on the polymerization using **Fe1**/MMAO was investigated with the Al:Fe ratio set at 2000 and the run time at 30 min. Inspection of the results (Table 2, entries 1 – 7) reveals the highest activity to be reached at 50 °C (up to 12.23×10^6 g(PE) mol^{-1} (Fe) h^{-1}) (entry 3, Table 2) with only modest decreases in activity evident at 40 °C or 60 °C highlighting the temperature stability of the catalyst. Indeed, even at 90 °C, the activity dropped to only 6.75×10^6 g(PE) mol^{-1}(Fe) h^{-1} (entry 7, Table 2). On the other hand, the molecular weight (M_w) of the resultant polyethylenes generated using **Fe1**/MMAO was found to decrease sharply from 168.9 to 35.9 kg·mol^{-1} on raising the temperature from 30 to 90 °C (Figure 3a), which may be attributed to either increased chain transfer to aluminum or chain termination by β-H elimination at the higher temperature.[4g-l,11a,12a,13,16a] Indeed, the molecular weight distribution for the polymeric materials ranges from bimodal (≤ 60 °C), with two M_{pk} peaks (peaks 1 and peak 2) clearly visible in their GPC spectra, to unimodal (≥ 70 °C) (Figure 3b).[18] Moreover, it is apparent that the lower molecular weight fraction of the distribution becomes the major component at higher temperature. A similar trend has been displayed for related catalysts.[4k]

Table 2 Polymerization screening using **Fe1** with MMAO as co-catalyst.[a]

Entry	Al:Fe	T (°C)	t (min)	Mass of PE (g)	Activity[b]	M_{pk}		M_w[c]	M_w/M_n[c]	T_m[d] (°C)
						Peak 1	*Peak 2*			
1	2000	30	30	4.37	2.91	74.5 (9%)	3.1 (91%)	168.9	29.1	131.1
2	2000	40	30	15.88	10.59	66.0 (44%)	3.0 (56%)	147.7	28.6	131.6
3	2000	50	30	18.34	12.23	61.2 (48%)	2.0 (52%)	133.7	34.1	131.1
4	2000	60	30	15.20	10.13	62.7 (23%)	2.1 (77%)	93.7	33.3	129.9
5	2000	70	30	14.62	9.75	3.2 (100%)		68.5	24.7	128.8
6	2000	80	30	12.57	8.38	2.3 (100%)		52.6	23.6	128.4
7	2000	90	30	10.13	6.75	2.5 (100%)		35.9	15.2	127.7
8	1500	50	30	16.46	10.97	77.9 (51%)	2.1 (49%)	151.3	33.9	132.2
9	1750	50	30	17.36	11.57	67.1 (58%)	2.4 (42%)	131.0	29.3	131.6
10	2250	50	30	17.75	11.83	58.2 (43%)	2.3 (57%)	85.8	30.3	129.3
11	2500	50	30	17.05	11.37	56.2 (42%)	2.1 (58%)	81.7	31.7	130.2
12	2000	50	5	8.45	33.80	2.0 (100%)		18.2	10.3	128.0
13	2000	50	15	13.36	17.81	2.1 (100%)		74.3	24.2	130.2
14	2000	50	45	18.95	8.42	74.5 (44%)	1.7 (56%)	134.5	45.4	130.8
15	2000	50	60	19.15	6.38	89.7 (51%)	2.7 (49%)	188.2	45.2	130.7
16[e]	2000	50	30	10.56	7.04	68.8 (48%)	1.1 (52%)	94.4	32.6	131.6
17[f]	2000	50	30	1.80	1.20	5.3 (42%)	1.2 (58%)	10.3	21.4	128.5

[a] Conditions: 3.0 µmol of **Fe1**, 100 mL toluene, 10 atm ethylene. [b] Values in units of 10^6 g(PE) mol^{-1} (Fe) h^{-1}. [c] Determined by GPC, and M_w: kg mol^{-1}. [d] Determined by DSC. [e] 5 atm ethylene. [f] 1 atm ethylene.

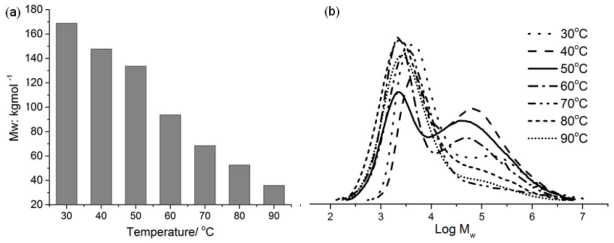

Figure 3 (a) Molecular weight as a function of temperature for the polyethylene obtained using **Fe1**/MMAO along with (b) the corresponding GPC curves (entries 1 – 7, Table 2)

Secondly, with the reaction temperature fixed at 50 °C, the Al:Fe molar ratio using **Fe1**/MMAO was varied between 1500 and 2500. Examination of the data indicates that there is little effect on the activity across this range in ratios (entries 3, 8 – 11, Table 2) with the standout value of 12.23 × 10^6 g(PE) mol^{-1} (Fe) h^{-1}) seen with an Al:Fe ratio of 2000 (entry 3, Table 2). By contrast, the molecular weight of the polymer was found to decrease by nearly half from 151.3 to 81.7 kg·mol^{-1} on changing the ratio from 1500 to 2500 (Figure 4a), which can be credited to increased chain transfer from the iron center to aluminum on increasing the amount of MMAO.[4e,4g-k,21] Similar behavior has been observed for related iron precatalysts containing **B**- and **F**-type ligand sets.[12a,16a] Indeed, a bimodal distribution was a feature of all these runs (Figure 4b) with the lower molecular weight fraction becoming more significant with larger amounts of alkyl aluminum reagent.[11a,12a,14a,16a]

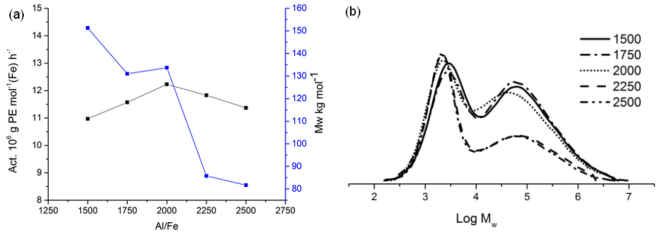

Figure 4 (a) Effect of Al:Fe molar ratio on the catalytic activity and molecular weight (M_w) of the polyethylene generated using **Fe1**/MMAO (entries 3, 8–11, Table 2); (b) GPC curves showing the variation of molecular weight with Al:Fe molar ratio

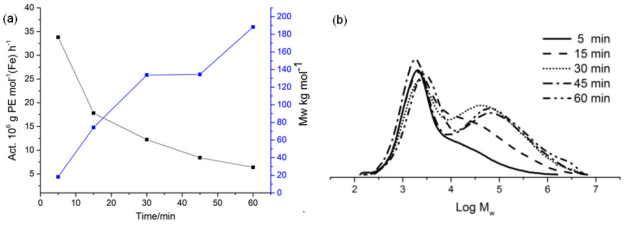

Figure 5 (a) Effect of time on the catalytic activity and molecular weight of the polyethylene produced using **Fe1**/MMAO (entries 3, 12–15, Table 2); (b) GPC curves showing the variation of molecular weight with time

Thirdly, to investigate the lifetime of the active species formed and the effect of the run time on the polymerization, the catalytic screens using **Fe1**/MMAO were conducted at time intervals between 5 and 60 min (entries 3 and 12 – 15, Table 2) with the Al:Fe ratio set at 2000 and the temperature at 50 °C. The highest activity of 33.80 × 10^6 g(PE) mol^{-1} (Fe) h^{-1} was observed at the 5 min mark (entry 12, Table 2) after which the activity gradually decreased reaching its lowest value of 6.38 × 10^6 g (PE) mol^{-1} (Fe) h^{-1} at 60 min (entry 15, Table 2). Notably, the activity after 5 min was more than twice that observed after 30 min (entry 2, Table 2), this observation would suggest that the active species formed quickly after the addition of MMAO and underwent gradual deactivation over time.[11,13-16,22] Conversely, the molecular weight of the polymers markedly increased over time and broad bimodal distributions were again a feature of all the polymers with the higher molecular weight fraction becoming the major component over more extended run times (Figure 5). On lowering the ethylene pressure from 10 to 5 atm the catalytic activity dropped by nearly a half (entry 16 *vs.* entry 3, Table 2). Meanwhile at 1 atm ethylene, the lowest activity (1.20 × 10^6 g(PE) mol^{-1} (Fe) h^{-1}) (entry 17 *vs.* entries 3 and 16, Table 2) was observed which is likely due to the lower ethylene concentration at lower pressure.[4g-h,11a,12a,14a,16a]

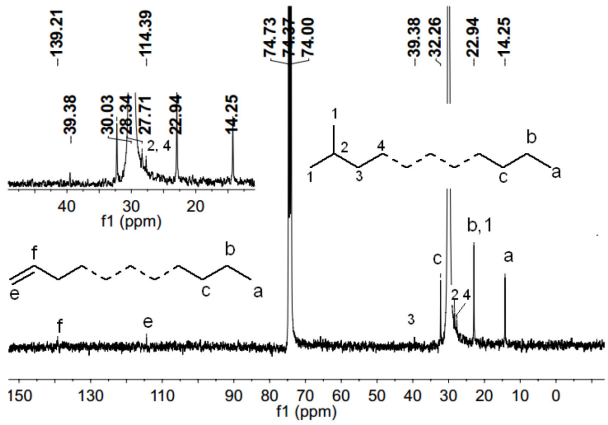

Figure 6 ^{13}C NMR spectrum of the polyethylene produced using **Fe1**/MMAO at 50 °C (recorded in 1,1,2,2-tetrachloroethane-d_2 at 135 °C) (entry 3, Table 2); an expansion of the upfield region is also shown.

To investigate the microstructural properties of the polyethylenes generated using **Fe1**/MMAO, both DSC and high temperature ^{13}C NMR spectroscopic measurements were employed. Generally, the melting temperatures of the polymers were close to or greater than 130 °C (Table 2) indicative of highly linear structures. In the case of the polymer obtained at 50 °C (entry 3, Table 2), the ^{13}C NMR spectrum (recorded at 100 °C in 1,1,2,2-tetrachloroethane-d_2) revealed a sharp singlet at δ 30.0 supporting the presence of equivalent -$(CH_2)_n$- repeat units.[2b,11a,12a,14a,16,18] In addition, low intensity peaks visible at δ 32.3, 22.9 and 14.3 can be ascribed to a *n*-propyl end-group (peaks a – c in Figure 5) while even weaker signals at δ 39.4, 28.3, 27.7 and 22.9 can be assigned to an *iso*-butyl end-group (peaks 1–4, Figure 6).[4a,4c] Furthermore, scrutiny of the more downfield region indicates weak signals at δ 139.2 and 114.4 which are characteristic of a vinyl-end group (peaks e and f in Fig. 6).[2b] This chain-end analysis would suggest that both chain transfer to aluminum and β-H elimination are operative while the relatively high amounts of *n*-propyl to *iso*-butyl end-groups indicates that catalyst has a preference to undergo termination by chain transfer to $AlMe_3$ rather than Al(*i*-Bu_3) and its derivatives present in MMAO.[4a,4c] Notably, a mechanism of this type has recently been proposed by Bryliakov *et al.* to account for a similar *iso*-butyl/*n*-

propyl chain-end combination which occurs at high concentrations of MMAO using bis(imino)pyridine-iron catalysts.[4a,4c] Overall, this ^{13}C NMR spectroscopic study suggests the bimodality observed in the GPC traces is due to variations in the chain termination processes as opposed to the existence of two types of catalytically active sites.

With the optimal conditions established for **Fe1**/MMAO [Al:Fe ratio of 2000, reaction temperature of 50 °C and run time of 30 min], the other precatalysts **Fe2** – **Fe5** and **Fe3'** were additionally screened for ethylene polymerization (entries 2 – 6, Table 3). All these iron complexes showed high activities (3.27 – 12.23 × 10^6 g(PE) mol^{-1} (Fe) h^{-1}) and produced highly linearly polyethylenes (T_m ≈ 131 °C) with broad distributions (M_w/M_n = 31.5 – 35.4) (entries 1 – 6, Table 3). With respect to the five ferrous precatalysts **Fe1** – **Fe5**, the activities fall in the order, **Fe1** [2,6-di(Me)] > **Fe4** [2,4,6-tri(Me)] > **Fe2** [2,6-di(Et)] > **Fe5** [2,6-di(Et)-4-Me] > **Fe3** [2,6-di(*i*-Pr)], while further examination of the data reveals two sub-trends namely **Fe1** [2,6-di(Me)] > **Fe2** [2,6-di(Et)] > **Fe3** [2,6-di(*i*-Pr)] and **Fe4** [2,4,6-tri(Me)] > **Fe5** [2,6-di(Et)-4-Me]. Overall these trends suggest that as the steric properties of the N-aryl groups increase, the coordination and insertion of ethylene is more and more impeded.[11a,12a,14a,16a,23] Indeed, the most hindered precatalyst **Fe3** (2,6-diisopropyl) displayed the lowest activity, but nevertheless produced the polyethylene with the highest molecular weight (entry 3, Table 3); similar findings have been reported for iron precatalysts ligated by **C**, **D** and **F** (Chart 1).[11a,12a,14a,16a] In comparison with the results obtained with **Fe3**/MMAO, diferric **Fe3'** on activation with MMAO exhibited a lower activity (up to 3.27 × 10^6 g(PE) mol^{-1} (Fe) h^{-1}) and produced polymer with lower molecular weight (entries 3 *vs* 6, Table 3); similar findings have been previously reported for iron(II) and iron(III) precatalysts ligated by 2-(benzimidazole)-6-(1-aryliminoethyl)pyridines.[6d,24] In addition, comparison of the activities of either **Fe1** [2,6-di(Me)] with **Fe4** [2,4,6-tri(Me)] or **Fe2** [2,6-di(Et)] with **Fe5** [2,6-di(Et)-4-Me] showed the *para*-methyl group to have a negative effect on the activity; an observation that has been noted elsewhere.[16a]

Table 3 Polymerization screening of **Fe1** – **Fe5** and **Fe3**' with MMAO as co-catalyst under optimal conditions.[a]

Entry	Precat.	Al:Fe	T (°C)	t (min)	Mass of PE (g)	Activity[b]	M_{pk}		M_w[c]	M_w/M_n[c]	T_m[d] (°C)
							Peak 1	*Peak 2*			
1	**Fe1**	2000	50	30	18.34	12.23	61.2 (48%)	2.0 (52%)	133.7	34.1	131.1
2	**Fe2**	2000	50	30	12.75	8.50	64.7 (38%)	1.9 (62%)	106.2	31.8	131.0
3	**Fe3**	2000	50	30	6.25	4.16	98.3 (59%)	2.4 (41%)	178.0	34.4	131.8
4	**Fe4**	2000	50	30	15.12	10.08	84.6 (63%)	2.1 (36%)	148.5	31.5	131.6
5	**Fe5**	2000	50	30	9.56	6.37	92.4 (42%)	3.2 (58%)	168.3	32.4	131.0
6	**Fe3'**	2000	50	30	4.90	3.27	65.1 (56%)	2.4 (44%)	116.2	35.3	129.8

[a] Conditions: MMAO:Fe = 2000:1, 3.0 µmol of iron precatalyst, temperature is 50 °C, the run time is 30 min, 100 mL toluene, 10 atm ethylene. [b] Values in units of 10^6 g(PE) mol^{-1} (Fe) h^{-1}. [c] Determined by GPC, and M_w: kg mol^{-1}. [d] Determined by DSC.

(b) *Catalytic evaluation using Fe1 – Fe5 and Fe3' with MAO as co-catalyst*. To explore the effect of co-catalyst on the polymerization, MAO was independently screened [initial conditions: 10 atm ethylene, Al:Fe molar ratio at 2000 and 30 min run time] with **Fe1** again employed as the test precatalyst; the results are collected in Table 4. On increasing the polymerization temperature from 30 to 90 °C (entries 1 – 7, Table 4), a peak in catalytic activity was achieved of 7.75 × 10^6 g(PE) mol^{-1}(Fe) h^{-1} at 80 °C, as compared to 50 °C with **Fe1**/MAO. As with **Fe1**/MMAO, the molecular weight of the resultant polymers was found to decrease gradually from 144.2 to 79.3 kg mol^{-1} on increasing the temperature (Figure 7a). This observation is similar to that previously reported for iron-containing **A**, **C**, **D** and **F** (Chart 1) and can be accredited to either increased chain transfer to aluminum or chain termination by β-H elimination at the higher temperature.[2b,11a,12a,14b,16a] Unlike the polymers obtained using **Fe1**/MMAO, the GPC curves obtained using **Fe1**/MAO the over the same 30 – 90 °C temperature range indicate the distributions to be more monomodal-like in appearance with the values of M_w/M_n relatively narrow at 8.0 – 13.6 (Figure 7b).

Subsequently, the effect of varying the Al:Fe molar ratio from 1500 to 2500 was examined with the temperature fixed at 80 °C and the run time at 30 min (entries 6 and 8 – 11, Table 4). The highest activity of 8.21 × 10^6 g (PE) $(mol)^{-1}$ (Fe) h^{-1} was achieved at an Al:Fe molar ratio of 2250. Additionally, it was noted that the molecular weight of the resulting polymers decreased by about a third from 140.6 to 53.9 kg·mol^{-1} (Figure 8a) on increasing the ratio from 1500 to 2500, which can be attributed to increased chain termination involving transfer from iron to aluminum with larger amounts of alkyl aluminum reagent.[4f,12a,14a,21] In comparison with the results

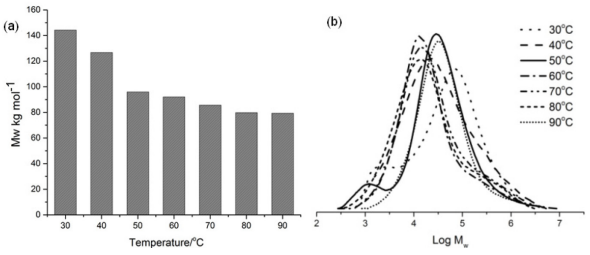

Figure 7 (a) Molecular weight of the polyethylene as a function of temperature using **Fe1**/MAO along with (b) the corresponding GPC curves (entries 1 – 7, Table 2)

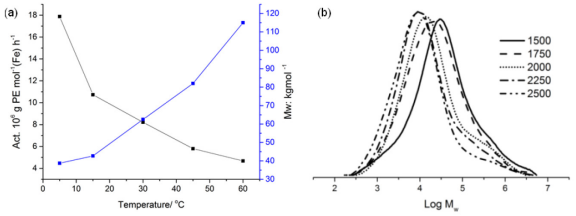

Figure 8 (a) Effect of temperature on the catalytic activity and molecular weight (M_w) of the polyethylene generated using **Fe1**/MAO (entries 6 and 8 - 11, Table 4); (b) GPC curves showing the variation of molecular weight with Al:Fe molar ratio

Journal Name

ARTICLE

Table 4 Optimization of the polymerization conditions using **Fe1**/MAO.[a]

Entry	Al:Fe	T (°C)	t (min)	Mass of PE (g)	Activity[b]	M_w[c]	M_w/M_n[c]	T_m[d] (°C)
1	2000	30	30	5.25	3.47	144.2	13.6	135.4
2	2000	40	30	7.89	5.26	126.8	9.4	134.7
3	2000	50	30	8.01	5.34	96.0	10.4	134.4
4	2000	60	30	9.94	6.27	92.1	9.8	134.5
5	2000	70	30	11.31	7.54	85.7	9.5	133.1
6	2000	80	30	11.62	7.75	79.8	10.5	133.7
7	2000	90	30	6.50	4.33	79.3	8.0	134.3
8	1500	80	30	9.56	6.37	140.6	15.2	133.1
9	1750	80	30	11.46	7.64	80.4	10.7	133.6
10	2250	80	30	12.32	8.21	62.5	11.2	131.8
11	2500	80	30	9.86	6.57	53.9	12.8	131.6
12	2250	80	5	4.47	17.88	38.7	9.58	130.5
13	2250	80	15	8.05	10.73	42.7	11.2	132.9
14	2250	80	45	13.05	5.80	82.0	10.5	133.3
15	2250	80	60	14.03	4.68	115.0	19.5	133.9
16[e]	2250	80	30	6.74	4.49	115.9	29.5	133.5
17[f]	2250	80	30	1.02	0.68	14.6	9.4	126.3

[a] Conditions: 3.0 µmol of **Fe1**, 100 mL toluene, 10 atm ethylene. [b] Values in units of 10^6 g(PE) mol^{-1} (Fe) h^{-1}. [c] Determined by GPC, and M_w: kg mol^{-1}. [d] Determined by DSC. [e] 5 atm ethylene. [f] 1 atm ethylene.

obtained with **Fe1**/MMAO, these MAO-promoted polymerizations was found to produce polymers that again displayed a narrower molecular weight distribution over the range in molar ratios (M_w/M_n = 10.7 – 15.4, Figure 8b).

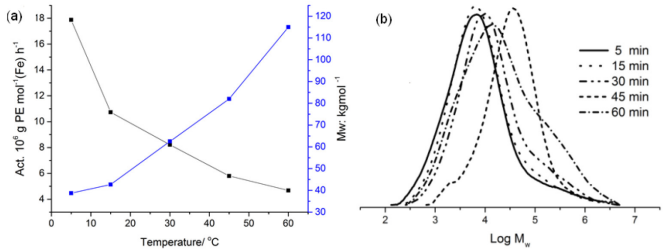

Figure 9 (a) Molecular weight and (b) GPC curves for the polyethylenes obtained using **Fe1**/MAO at different run times (entries 10 and 12 - 15, Table 4)

With the temperature set at 80 °C and the Al:Fe ratio at 2250, the lifetime of **Fe1**/MAO was studied by conducting the polymerization over 5, 15, 30, 45 and 60 min (entries 10 and 12 – 15, Table 4). The highest activity of 17.88 × 10^6 g(PE) $(mol)^{-1}$ Fe h^{-1} was achieved over 5 min after which it progressively decreased reaching its lowest value of 4.68 × 10^6 g(PE) $(mol)^{-1}$ Fe h^{-1} after 60 min (Figure 9a). In terms of molecular weight (Figure 9b), this was found to increase with run time reaching a maximum of 115.0 kg mol^{-1} after 60 min (entry 15, Table 4). Reducing the ethylene pressure to 5 atm (entry 16, Table 3; 30 minutes run time) resulted in a drop in activity (4.49 × 10^6 g(PE) $(mol)^{-1}$ Fe h^{-1}) (entry 16 *vs.* entry 10, Table 4), while at ambient pressure the activity was almost twelve times less than that observed at 10 atm (entry 17 *vs.* entry 10, Table 4). Such pressure effects can be attributed to the lower solubility of ethylene in toluene at an ambient ethylene pressure as compared to that at higher pressure.[14a,16a,16b]

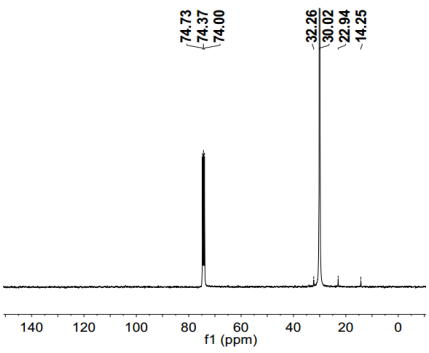

Figure 10 ^{13}C NMR spectrum of the polyethylene obtained with **Fe1**/MAO at 80 °C (recorded at 135 °C in 1,1,2,2-tetrachloroethane-d_2) (entry 10, Table 4).

To compare the microstructural properties of the polymer obtained using **Fe1**/MMAO at 50 °C (*vide supra*), the high temperature ^{13}C NMR spectrum was also recorded [at 135 °C in deuterated 1,1,2,2-tetrachloroethane-d_2] of the polyethylene obtained using **Fe1**/MAO at 80 °C (entry 10, Table 4). The spectrum reveals a high intensity peak around δ 30.2 consistent with a highly

linear polyethylene (Figure 10),[2b,11,12,14,16,18] which is further corroborated by its high melting temperature (T_m = 131.8 °C, entry 10, Table 4). Lower intensity peaks at 32.3, 22.9 and 14.3 are also visible which are characteristic of a *n*-propyl end-group (Figure 10).[4a,4c,18] Unlike that seen with **Fe1**/MMAO, no evidence of unsaturated chain ends could be detected which is consistent with the absence of any significant chain termination via β-H elimination.

Finally, using the optimized conditions established for **Fe1** [Al:Fe ratio = 2250, run temp = 80 °C and run time = 30 min], the performance of the remaining precatalysts, **Fe2** – **Fe5** and **Fe3'** was also studied; the results are collected in Table 5. In general, the iron(II) precatalyts **Fe2** – **Fe5** showed high activity (2.86 – 7.10 × 10^6 g(PE) mol^{-1} (Fe) h^{-1}) and the resulting linear polyethylenes displayed broad mono-modal molecular weight distributions (M_w/M_n = 11.2 – 21.3). As with the MMAO tests, those performed with MAO exhibit a similar trend in activities, **Fe1** [2,6-di(Me)] > **Fe4** [2,4,6-tri(Me)] > **Fe2** [2,6-di(Et)] > **Fe5** [2,6-di(Et)-4-Me] > **Fe3** [2,6-di(i-Pr)], with the least sterically bulky **Fe1** and **Fe4** showing higher activity than the more bulky analogues, **Fe2**, **Fe3** and **Fe5**. Similarly, the iron(III)-containing **Fe3'** exhibited lower activity (up to 2.48 × 10^6 g (PE) mol^{-1} (Fe) h^{-1}) and produced polymer with the lower molecular weight (entries 3 *vs* 6, Table 5) than that seen using **Fe3**.

Table 5 Screening of **Fe1** – **Fe5** and **Fe3'** with MAO under optimal conditions.[a]

Entry	Precat.	Al:Fe	T (°C)	t (min)	Mass of PE (g)	Activity[b]	M_w[c]	M_w/M_n[c]	T_m[d] (°C)
1	**Fe1**	2250	80	30	12.32	8.21	62.5	11.2	131.8
2	**Fe2**	2250	80	30	7.67	5.11	63.4	17.4	130.4
3	**Fe3**	2250	80	30	4.24	2.86	186.5	20.7	134.2
4	**Fe4**	2250	80	30	10.65	7.10	114.4	21.3	132.4
5	**Fe5**	2250	80	30	6.28	4.19	138.4	14.5	133.2
6	**Fe3'**	2250	80	30	3.72	2.48	127.3	25.4	128.9

[a] Conditions: MAO:Fe = 2250:1, 3.0 µmol of iron precatalyst, temp is 80 °C, run time is 30 min, 100 mL toluene, 10 atm ethylene.

[b] Values in units of 10^6 g(PE) mol^{-1} (Fe) h^{-1}. [c] Determined by GPC, and M_w: kg mol^{-1}. [d] Determined by DSC.

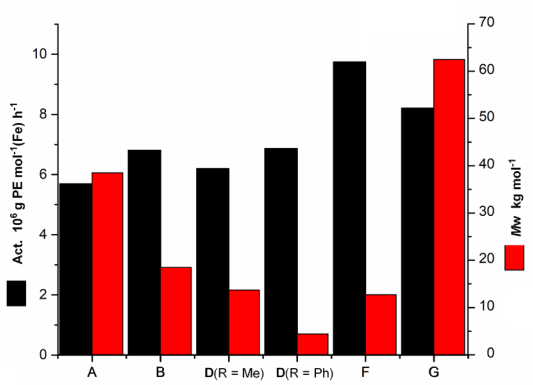

Figure 11 Comparison of the catalytic performance of (**G**)$FeCl_2$ (**Fe1**) with (**A**)$FeCl_2$,[4a] (**B**)$FeCl_2$,[12a] ($\mathbf{D}_{Me}$)$FeCl_2$ (R = Me),[14a] ($\mathbf{D}_{Ph}$)$FeCl_2$ (R = Ph)[11a] and (**F**)$FeCl_2$[16a] at 80 °C (see Chart 1); runs all performed at 80 °C with MAO used as activator.

Given the good performance characteristics of this family of iron catalyst at high temperature, it was of interest to compare them with other iron precatalysts that have been screened at 80 °C using otherwise comparable conditions. In this regard iron(II) complexes bearing the *N,N,N* ligands **A**[2b,4b], **B**,[12a] **D** (R = Me),[14a] **D** (R = Ph)[11a] and **F**[16a] (Chart 1) have all been reported with MAO as the co-catalyst using a related screening protocol (Tables S1 - S5, Figure 11). Inspection of Figure 11 reveals that in terms of catalytic activity, (**G**)$FeCl_2$ (**Fe1**) is second only to that seen with (**F**)$FeCl_2$.[16a] On the other hand, the molecular weight of the polyethylene obtained using (**G**)$FeCl_2$ (62.5 kg mol^{-1}) far exceeds that generated using (**A**)$FeCl_2$,[2b,4a] (**B**)$FeCl_2$,[12a] ($\mathbf{D}_{Me}$)$FeCl_2$ (R = Me),[14a] ($\mathbf{D}_{Ph}$)$FeCl_2$ (R = Ph)[11a] and (**F**)$FeCl_2$.[16a] It is unclear as to the precise origin of these outstanding performance characteristics displayed by (**G**)$FeCl_2$, but it is likely due to the superior chelation properties of this ligand manifold leading to a more thermally stable catalytic species. Even at high operating temperature the requisite steric protection is maintained so as to inhibit chain termination leading to high molecular weight polymer.

Conclusions

Iron(II) chloride chelates, **Fe1** – **Fe5**, each bearing one sterically and electronically distinct α,α'-bis(arylimino)-2,3:5,6-bis(hexamethylene) -pyridine, have been synthesized in good yield using straightforward one-pot strategies. All complexes on activation with either modified methylaluminoxane (MMAO) or methylaluminoxane (MAO), behaved as exceptionally active catalysts displaying levels as high as 12.23 × 10^6 g (PE) mol^{-1} (Fe) h^{-1} at 50 °C. Even with the temperature at 80 °C, **Fe1**/MAO still maintained high activity (8.21 × 10^6 g(PE) mol^{-1} (Fe) h^{-1}) generating strictly linear polyethylenes with high molecular weight. Compared to the results obtained with **Fe3**, iron(III)-containing **Fe3'** exhibited lower activities and produced the polymers with lower molecular weight. With regard to the steric properties of the precatalyst, the least sterically hindered **Fe1** (R^1 = Me) and **Fe4** (R^1 = Me) exhibit higher activity than their bulkier counterparts **Fe2** (R^1 = Et), **Fe3** (R^1 = *i*-Pr) and **Fe5** (R^1 = Et). In terms of electronic variations, the *para*-methyl containing **Fe4** and **Fe5** are less active than their *para*-proton containing analogues **Fe1** and **Fe2**. Additionally, with MMAO as co-catalyst the resulting polyethylenes display bimodal distributions with both unsaturated vinyl-end groups and saturated *n*-propyl and *i*-butyl chain ends a feature; the co-existence of two chain termination processes namely chain transfer to aluminum and β-H elimination has been offered as an explanation. On the other, with MAO as the co-catalyst, a relatively narrow distribution for the polymer is apparent (M_w/M_n = 8.0 – 19.5).

Experimental Section

General Considerations. All manipulations involving air and moisture sensitive compounds were carried out under a nitrogen atmosphere by using standard Schlenk techniques. Toluene was heated to reflux over sodium and distilled under nitrogen prior to use. MAO (1.46 M solution in toluene) and MMAO (1.93 M in *n*-heptane) were purchased from Akzo Nobel Corp. High-purity ethylene was purchased from Beijing Yansan Petrochemical Co. and used as received. Other reagents were purchased from Aldrich, Acros or local suppliers. NMR spectra were recorded with a Bruker DMX 400 MHz instrument at ambient temperature using TMS as the internal standard. IR spectra were recorded with a Perkin Elmer System 2000 FTIR spectrometer. Elemental analysis was carried out with a Flash EA 1112 microanalyzer. Molecular weights and molecular weight distributions of the polyethylenes were determined with an Agilent PL-GPC 220 GPC/SEC system at 150 °C with 1,2,4-trichlorobenzene as solvent. The columns used were three 300 × 7.5 mm PLgel 10 µm MIXED-B LS columns connected in series. The testing was undertaken at 150 °C with a flow rate of 1.0 ml min^{-1} with 1,2,4-trichlorobenzene (TCB) as eluent. The samples were dissolved at a concentration of 0.5 to 2.5 mg ml^{-1}, depending on the molecular weights.[14b] The data were collected every second and processed using Cirrus GPC Software and Multi Detector Software with the standard of Polystyrene Calibration KitS-M-10 from PL Company. The melting temperatures of the polyethylenes were measured from the fourth scanning run on a Perkin Elmer TA-Q2000 differential scanning calorimeter under a nitrogen atmosphere. A sample of about 5.0 mg was heated to 140 °C at a rate of 20 °C min^{-1}, kept for 2 min at 140 °C to remove the thermal history and then cooled to –40 °C at a rate of 20 °C min^{-1}. ^{13}C NMR spectra of the polyethylenes were recorded with a Bruker DMX 300 MHz instrument at 135 °C in 1,1,2,2-tetrachloroethane-d_2 with TMS as internal standard. The compound α,α′-dioxo-2,3:5,6-bis(hexam-ethylene)pyridine was prepared using a previously reported procedure.[18]

Preparation of [2,3:5,6-{$C_5H_{10}C(NAr)$}$_2C_5HN$]$FeCl_2$

(a) Ar = 2,6-$Me_2C_6H_3$ (**Fe1**). A suspension of α,α′-dioxo-2,3:5,6-bis(hexamethylene)pyridine (0.27 g, 1.0 mmol), 2,6-dimethylaniline (0.48 g, 4.0 mmol) and $FeCl_2{\cdot}4H_2O$ (0.19 g, 1.0 mol) in glacial acetic acid (15 mL) was stirred and heated to reflux for 12 h. On cooling to room temperature, an excess of diethyl ether was added to precipitate the crude product which was collected before being re-dissolved in methanol (5 mL). The methanol solution was concentrated and the product again precipitated with diethyl ether. Following filtration and drying under reduced pressure **Fe1** was obtained as a blue powder (0.49 g, 89%). FT-IR (cm^{-1}): 2928 (m), 2859 (w), 1591 (m, $\nu_{C=N}$), 1535 (w), 1448 (s), 1376 (w), 1311 (w), 1256 (w), 1225 (w), 1203 (m), 1162 (w), 1095 (w), 1031 (w), 924 (w), 839 (w), 768 (s), 700 (w). Anal. Calcd for $C_{33}H_{39}Cl_2FeN_3$ (604.44): C, 65.58, H, 6.50, N, 6.95; found C 65.23, H, 6.70, N, 6.83%.

(b) Ar = 2,6-$Et_2C_6H_3$ (**Fe2**). By using a similar one-pot approach to that described for of **Fe1**, **Fe2** was obtained as a blue powder (0.45 g, 75%). FT-IR (cm^{-1}): 2929 (m), 2860 (w), 1599 (m, $\nu_{C=N}$), 1537 (w), 1447 (s), 1310 (w), 1252 (m), 1225 (w), 1195 (w), 1158 (w), 1036 (w), 1009 (w), 924 (w), 839 (w), 806 (m), 758 (s), 695 (w). Anal. Calcd for $C_{37}H_{47}Cl_2FeN_3$ (660.55): C, 67.28, H, 7.17, N, 6.36; found C 67.13, H, 7.22, N, 6.23%.

(c) Ar = 2,6-i-$Pr_2C_6H_3$ (**Fe3**). By using a similar one-pot approach to that described for the synthesis of **Fe1**, **Fe3** was obtained as a blue powder (0.56 g, 86%). FT-IR (cm^{-1}): 2927 (m), 2861 (w), 1597 (m, $\nu_{C=N}$), 1446 (s), 1312 (w), 1252 (s), 1197 (w), 1163 (w), 1040 (w), 926 (w), 840 (w), 756 (s). Anal. Calcd for $C_{41}H_{55}Cl_2FeN_3$ (716.66): C, 68.72, H, 7.74, N, 5.86; found C, 68.52, H, 7.84, N, 5.76%.

(d) Ar = 2,4,6-$Me_3C_6H_2$ (**Fe4**). By using a similar one-pot approach to that described for the synthesis of **Fe1**, **Fe4** was obtained as a blue powder (0.50 g, 88%). FT-IR (cm^{-1}): 2923 (m), 2859 (w), 1604 (m, $\nu_{C=N}$), 1537 (w), 1447 (s), 1370 (w), 1310 (w), 1287 (m), 1225 (m), 1177 (w), 1037 (w), 969 (w), 859 (s), 737 (w). Anal. Calcd for $C_{35}H_{43}Cl_2FeN_3$ (632.50): C, 66.46, H, 6.85, N, 6.64; found: C 66.26, H, 6.96, N, 6.56%.

(e) Ar = 4-Me-2,6-$Et_2C_6H_3$ (**Fe5**). By using a similar one-pot approach to that described for the synthesis of **Fe1**, **Fe5** was obtained as a blue powder (0.54 g, 87%). FT-IR (cm^{-1}): 2927 (m), 2858 (w), 1602 (m, $\nu_{C=N}$), 1541 (w), 1448 (s), 1386 (w), 1350 (w), 1310 (w), 1230 (m), 1175 (w), 1114 (w), 1068 (w), 1036 (w), 922 (w), 856 (s), 782 (m), 743 (w). Anal. Calcd for $C_{39}H_{51}Cl_2FeN_3$ (688.60): C, 68.03, H, 7.47, N, 6.10; found: C, 67.93, H, 7.51, N, 6.13%.

Oxidation of Fe3 to form [2,3:5,6-{$C_5H_{10}C(N(2,6\text{-}i\text{-}Pr_2Ph))$}$_2$ C_5HN]$FeCl(\mu\text{-}O)FeCl_3$ (Fe3')

A sample of **Fe3** (0.35 g, 0.5 mmol) in dichloromethane (25 mL) was stirred for 24 h at 20 °C under an atmosphere of oxygen (or 120 hours under air) resulting in a color change of the solution from blue to light green. The solvent was removed under reduced pressure and diethyl ether (20 mL) added to induce precipitation. The solid was filtered, washed with diethyl ether and dried under reduced pressure affording [2,3:5,6-{$C_5H_{10}C(N(2,6\text{-}i\text{-}Pr_2Ph))$}$_2C_5HN$]$FeCl(\mu\text{-}O)FeCl_3$ (**Fe3'**) as a yellow solid (0.18 g, 84%). FT-IR (cm^{-1}): 2963 (m), 2929 (m), 2864 (w), 1677 (m, $\nu_{C=N}$) 1584 (m), 1543 (w), 1453 (s), 1385 (w), 1360 (w), 1306 (w), 1248 (m), 1188 (w), 1162 (w), 1110 (w), 1052 (w), 1009 (w), 932 (w), 844 (w, $\nu_{Fe\text{-}O\text{-}Fe}$), 799 (m), 754 (m). Anal. Calcd for $C_{41}H_{55}Cl_4Fe_2N_3O$ (859.40): C, 57.30, H, 6.45, N, 4.89; found: C, 57.22, H, 6.23, N, 4.70%.

Polymerization studies

Ethylene polymerization at P_{C2H4} = 5 or 10 atm

The autoclave was evacuated and backfilled with ethylene three times. When the required temperature was reached, the precatalyst (3 µmol) was dissolved in toluene (30 mL) in a Schlenk tube and injected into the autoclave containing ethylene (~ 1 atm) followed by the addition of more toluene (30 mL). The required amount of co-catalyst (MAO and MMAO) and additional toluene were added successively by syringe taking the total volume of toluene to 100 mL. The autoclave was immediately pressurized with 5/10 atm. pressure of ethylene and the stirring commenced. After the required reaction time, the reactor was cooled with a water bath and the excess ethylene vented. Following quenching of the reaction with 10% hydrochloric acid in ethanol, the polymer

was collected and washed with ethanol and dried under reduced pressure at 50 °C and weighed.

Ethylene polymerization at P_{C2H4} = 1 atm

The polymerization at 1 atm ethylene pressure was carried out in a Schlenk tube. Under an ethylene atmosphere (1 atm), **Co4** (3.0 μmol) was added followed by toluene (30 mL) and then the required amount of co-catalyst (MAO, MMAO) introduced by syringe. The solution was then stirred at 40 °C under an ethylene atmosphere (1 atm). After 30 min, the solution was quenched with 10% hydrochloric acid in ethanol. The polymer was washed with ethanol, dried under reduced pressure at 40 °C and then weighed.

X-ray structure determinations

Single-crystal X-ray diffraction studies of **Fe3** and **Fe3'** were conducted on a Rigaku Sealed Tube CCD (Saturn 724+) diffractometer with graphite-mono chromated Mo-Kα radiation (λ = 0.71073 Å) at 173(2) K and the cell parameters obtained by global refinement of the positions of all collected reflections. Intensities were corrected for Lorentz and polarization effects and empirical absorption. The structures were solved by direct methods and refined by full-matrix least-squares on F^2. All non-hydrogen atoms were refined anisotropically and all hydrogen atoms were placed in calculated positions. Structure solution and refinement were performed by using the SHELXT (Sheldrick, 2015).[25] The disorder displayed by the Cl atoms in **Fe3'** was processed by the SHELXL-97 software.[25b] Crystal data and processing parameters for **Fe3** and **Fe3'** are summarized in Table S6.

Conflicts of interest

There are no conflicts to declare.

Acknowledgements

This work was supported by the National Natural Science Foundation of China (No. 21871275, 51473170 and 51273202). G.A.S. thanks the Chinese Academy of Sciences for a President's International Fellowship for Visiting Scientists.

Notes and references

1. (a) B. L. Small, M. Brookhart, and A. M. A. Bennett, *J. Am. Chem. Soc.*, 1998, **120**, 4049–4050; (b) B. L. Small, M. Brookhart, *J. Am. Chem. Soc*., 1998, **120**, 7143−7144.
2. (a) G. J. P. Britovsek, V. C. Gibson, B. S. Kimberley, P. J. Maddox, S. J. McTavish, G. A. Solan, A. J. P. White, and D. J. Williams, *Chem. Commun*., 1998, 849–850; (b) G. J. P. Britovsek, M. Bruce, V. C. Gibson, B. S. Kimberley, P. J. Maddox, S. Mastroianni, S. J. McTavish, C. Redshaw, G. A. Solan, S. Stromberg, A. J. P. White, and D. J. Williams, *J. Am. Chem. Soc*., 1999, **121**, 8728–8740; (c) G. J. P. Britovsek, S. Mastroianni, G. A. Solan, S. P. D. Baugh, C. Redshaw, V. C. Gibson, A. J. P. White, D. J. Williams, M. R. Elsegood. *Chem. Eur. J*. 2000, **6**, 2221–2231; (d) G. J. P. Britovsek, V. C. Gibson, B. S. Kimberley, S. Mastroianni, C. Redshaw, G. A. Solan, A. J. P. White, D. J. Williams, *J. Chem. Soc., Dalton Trans*. 2001, 1639–1644; (e) G. J. P. Britovsek, V. C. Gibson, S. K. Spitzmesser, K. P. Tellmann, A. J. P. White, D. J. Williams, *J. Chem. Soc., Dalton Trans*. 2002, 1159–1171.
3. For reviews see: (b) Z. Wang, G. A. Solan, W. Zhang, and W.-H. Sun, *Coord. Chem. Rev*. 2018, **363**, 92–108; (b) B. L. Small, *Acc. Chem. Res*., 2015, **48**, 2599–2611; (c) B. Burcher, P. -A. R. Breuil, L. Magna, and H. Olivier-Bourbigou, *Top Organomet Chem.* 2015, **50**, 217–258; (d) Z. Flisak, W.-H. Sun, *ACS Catal*. 2015, **5**, 4713–4724; (e) J. Ma, C. Feng, S. Wang, K. -Q. Zhao, W. -H. Sun, C. Redshaw, G. A. Solan, *Inorg. Chem. Front*. 2014, **1**, 14–34; (f) W. Zhang, W. -H. Sun, C. Redshaw, *Dalton Trans*. 2013, **42**, 8988–8997; (g) V. C. Gibson, G. A. Solan, in Catalysis without Precious Metals (Ed. R. M. Bullock), Wiley-VCH, Weinheim, 2010, 111–141; (h) V. C. Gibson, G. A. Solan, *Top. Organomet. Chem*. 2009, **26**, 107–158; (i) V. C. Gibson, C. Redshaw, G. A. Solan, *Chem. Rev*. 2007, **107**, 1745–1776; (j) C. Bianchini, G. Giambastiani, I. G. Rios, G. Mantovani, A. Meli, A. M. Segarra, *Coord. Chem. Rev*. 2006, **250**, 1391–1418
4. (a) Q. Mahmood, J. Guo, W. Zhang, Y. Ma, T. Liang, and W.-H. Sun, *Organometallics* 2018, **37**, 957–970; (b) Q. Mahmood, E. Yue, J. Guo, W. Zhang, Y. Ma, X. Hao, W.-H. Sun, Polymer, 2018, **159**, 124–137; (c) N. V. Semikolenova, W.-H. Sun, I. E. Soshnikov, M. A. Matsko, O. V. Kolesova, V. A. Zakharov, K. P. Bryliakov, *ACS Catal.*, 2017, **7**, 2868–2877; (d) W. Zhao, E. Yue, X. Wang, W. Yang, Y. Chen, X. Hao, X. Cao, W.-H. Sun, *J. Polym. Sci., Part A: Polym. Chem*., 2017, **55**, 988–996; (e) N. E. Mitchell, W. C. Anderson, B. K. Long, *J. Polym. Sci., Part A: Polym. Chem*., 2017, **55**, 3990–3996; (f) E. Yue, Y. Zeng, W. Zhang, Y. Sun, X.-P. Cao, W.-H. Sun, *Sci. China Chem*. 2016, **59**, 1291–1300; (g) W. Zhang, S. Wang, S. Du, C.-Y. Guo, X. Hao, W.-H. Sun, *Macromol. Chem. Phys.* 2014, **215**, 1797–1809; (h) S. Wang, B. Li, T. Liang, C. Redshaw, Y. Li, W.-H. Sun, *Dalton Trans.* 2013, **42**, 9188–9197; (i) T. M. Smit, A. K. Tomov, G. J. P. Britovsek, V. C. Gibson, A. J. P. White, D. J. Williams, *Catal. Sci. Technol*., 2012, **2**, 643–655; (j) W. Zhao, J. Yu, S. Song, W. Yang, H. Liu, X. Hao, C. Redshaw, W.-H. Sun, *Polymer* 2012, **53**, 130–137; (k) X. Cao, F. He, W. Zhao, Z. Cai, X. Hao, T. Shiono, C. Redshaw, W.-H. Sun, *Polymer* 2012, **53**, 1870–1880; (l) J. Lai, W. Zhao, W. Yang, C. Redshaw, T. Liang, Y. Liu, W.-H. Sun, *Polym. Chem.* 2012, **3**, 787 -793; (m) F. He, W. Zhao, X.-P. Cao, T. Liang, C. Redshaw, W.-H. Sun, *J. Organomet. Chem.* 2012, **713**, 209–216; (n) J. Yu, W. Huang, L. Wang, C. Redshaw, W. -H. Sun, *Dalton Trans*. 2011, **40**, 10209–10214; (o) J. Yu, H. Liu, W. Zhang, X. Hao, W.-H. Sun, *Chem Comm*., 2011, **47**, 3257–3259; (p) L. Guo, H. Gao, L. Zhang, F. Zhu, Q. Wu, *Organometallics* 2010, **29**, 2118–2125; (q) F. Kaul, K. Puchta, G. Frey, E. Herdtweck, W. Herrmann, *Organometallics* 2007, **26**, 988–999; (r) G. J. P. Britovsek, V. C. Gibson, O. D. Hoarau, S. K. Spitzmesser, A. J. P. White, D. J. Williams, *Inorg. Chem*. 2003, **42**, 3454–3465.
5. (a) L. Wang, W.-H. Sun, L. Han, H. Yang, Y. Hu, X. Jin, *J. Organomet. Chem*., 2002, **658**, 62–70; (b) W. -H. Sun, S. Jie, S. Zhang, W. Zhang, Y. Song, H. Ma, *Organometallics*, 2006, **25**, 666–677; (c) J. D. A. pelletier, Y. D. M. Champouret, J. Cardaso, L. Clowes, M. Gañete, K. Singh, V. Thanarajasingham, G. A. Solan, *J. Organomet. Chem*., 2006, **691**, 4114–4123; (d) S. Jie, S. Zhang, K. Wedeking, W. Zhang, H. Ma, X. Lu, Y. Deng, W.-H. Sun, *C. R. Chim*., 2006, **9**, 1500–1509; (e) S. Jie, S. Zhang, W. -H. Sun, X. Kuang, T. Liu, J. Guo, *J. Mol. Catal. A: Chem*., 2007, **269**, 85–96; (f) S. Jie, S. Zhang, W.-H. Sun, *Eur. J. Inorg. Chem*., 2007, **35**, 5584–5598; (g) M. Zhang, P. Hao, W. Zuo, S. Jie, W.-H. Sun, *J. Organomet. Chem.,* 2008, **693**, 483–491; (h) M. Zhang, R. Gao, X. Hao, W.-H. Sun, *J. Organomet. Chem*., 2008, **693**, 3867–3877; (f) M. Zhang, W. Zhang, T. Xiao, J.-F. Xiang, X. Hao, W.-H. Sun, *J. Mol. Catal. A -Chem*. 2010, **320**, 92-96.
6. (a) L. Xiao, R. Gao, M. Zhang, Y. Li, X. Cao, and W.-H. Sun, *Organometallics*, 2009, **28**, 2225–2233; (b) R. Gao, Y. Li, F. Wang, W.-H. Sun, and M. Bochmann, *Eur. J. Inorg. Chem.*, 2009, 4149–4156; (c) Y. Chen, P. Hao, W. Zuo, K. Gao, and W.-

H. Sun, *J. Organomet. Chem.,* 2008, **693**, 1829–1840; (d) W. -H. Sun, P. Hao, S. Zhang, Q. Shi, W. Zuo, X. Tang and X. Lu, *Organometallics*, 2007, **26**, 2720–2734; (e) Y. Huang, R. Zhang, T. Liang, X. Hu, G. A. Solan, and W.-H. Sun, Organometallics, 2019, **38**,1143−1150.

7. K. Wang, K. Wedeking, W. Zuo, D. Zhang, W.-H. Sun, *J. Organomet. Chem*., 2008, **693**, 1073–1080.
8. S. Zhang, W.-H. Sun, T. Xiao, X. Hao, *Organometallics*, 2010, **29**, 1168–1173.
9. Q. Knijnenburg, S. Gambarotta, and P. H. M. Budzelaar, *Dalton Trans*., 2006, 5442–5448.
10. (a) M. W. Bouwkamp, E. Lobkovsky, and P. J. Chirik, *Inorg. Chem*., 2006, **45**, 2–4; (b) H. Sugiyama, G. Aharonian, S. Gambarotta, G. P. A. Yap, P. H. M. Budzelaar, *J. Am. Chem. Soc*., 2002, **124**, 12268–12274.
11. (a) Y. Zhang, H. Suo, F. Huang, T. Liang, X. Hu, W.-H. Sun, *J. Polym. Sci. Part A. Polym.Chem*., 2017, **55**, 830–842; (b) F. Huang, W. Zhang, Y. Sun, X. Hu, G. A. Solan, W. H. Sun, *New J. Chem.* 2016, **40**, 8012–8023.
12. (a) W. Zhang, W. Chai, W.-H. Sun, X. Hu, C. Redshaw, X. Hao, *Organometallics*, 2012, **31**, 5039–5048; (b) W.-H. Sun, S. Kong, W. Chai, T. Shiono, C. Redshaw, X. Hu, C. Guo, X. Hao, *Appl. Catal.*, A, 2012, **447**–**448**, 67–73.
13. (a) J. Ba, S. Du, E. Yue, X. Hu, Z. Flisak, W.-H. Sun, *RSC Adv.*,2015, **5**, 32720–32729; (b) Y. Zhang, C. Huang, X. Hao, X. Hu, W.-H. Sun, *RSC Adv*., 2016, **6**, 91401–91408.
14. (a) F. Huang, Q. Xing, T. Liang, Z. Flisak, B. Ye, X. Hu, W. Yang, W.-H. Sun, *Dalton Trans*., 2014, **43**, 16818–16829; (b) F. Huang, W. Zhang, E. Yue, T. Liang, X. Hu, W.-H. Sun, *Dalton Trans*., 2016, **45**, 657–666.
15. V. K. Appukuttan, Y. Liu, B. C. Son, C.-S. Ha, H. Suh, I. Kim, *Organometallics*, 2011, **30**, 2285–2294.
16. (a) S. Du, X. Wang, W. Zhang, Z. Flisak, Y. Sun, W.-H. Sun, *Polym. Chem*., 2016, **7**, 4188–4197; (b) S. Du, W. Zhang, E. Yue, F. Huang, T. Liang, W.-H. Sun, *Eur. J. Inorg. Chem*., 2016, 1748–1755; (c) C. Huang, S. Du, G. A. Solan, Y. Sun, W.-H. Sun, *Dalton Trans.*, 2017, **46**, 6948–6957; (d) H. Suo, I. I. Oleynik, C. Bariashir, I. V. Oleynik, Z. Wang, G. A. Solan, Y. Ma, T. Liang, W.-H. Sun, *Polymer*, 2018, **149**, 45-54; (e) C. Bariashir, Z. Wang, H. Suo, M. Zada, G. A. Solan, Y. Ma, T. Liang, W.-H. Sun, *Eur. Polym. J.*, 2019, **110**, 240–251; (f) Z. Wang, Y. Ma, J. Guo, Q. Liu, Y. Sun, G. A. Solan, T. Liang, and W.-H. Sun, *Dalton Trans.,* 2019*,* **48**, 2582-2591.
17. (a) D. H. Camacho, E. V. Salo, J. W. Ziller, Z. Guan, *Angew. Chem. Int. Ed*. 2004, **43** 1821–1825; (b) C. S. Popeney, A. L. Rheingold, Z. Guan, *Organometallics* 2009, **28** 4452–4463; (c) D. H. Camacho, E. V. Salo, Z. Guan, J. W. Ziller, *Organometallics* 2005, **24**, 4933–4939; (d) D. H. Leung, J. W. Ziller, Z. Guan, *J. Am. Chem. Soc*. 2008, **130**, 7538–7539.
18. Wang, G. A, Solan, Q. Mahmood, Q. Liu, X. Hao, and W.-H. Sun, *Organometallics,* 2018, **37**, 380–389.
19. (a) D. M. Jr Kurtz, *Chem. Rev.*, 1990, **90**, 585–606; (b) B. L. Small, M. Brookhart, *Macromolecules* 1999, **32**, 2120-2130.
20. C. Bariashir, Z. Wang, S. Du, G. A. Solan, C. Huang, T. Liang, and W.-H. Sun, *J. Polym. Sci., Part A: Polym. Chem*., 2017, **55**, 3980–3989.
21. (a) D. J. Jones, V. C. Gibson, S. M. Green, P. J. Maddox, A. J. P. White, D. J. Williams, *J. Am. Chem.* Soc. 2005, **127**, 11037–11046; (b) A. K. Tomov, V. C. Gibson, G. J. P. Britovsek, R. J. Long, M. van Meurs, D. J. Jones, K. P. Tellmann, J. J. Chirinos, *Organometallics* 2009, **28**, 7033–7040.
22. T. Xiao, P. Hao, G. Kehr, X. Hao, G. Erker, W.-H. Sun, *Organometallics* 2011, **30**, 4847–4853.
23. (a) A. S. Abu-Surrah, K. Lappalainen, U. Piironen, P. Lehmus, T. Repo, M. Leskela, *J. Organomet. Chem*. 2002, **648**, 55–61; (b) W.-H. Sun, X. Tang, T. Gao, B. Wu, W. Zhang, H. Ma, *Organometallics* 2004, **23**, 5037–5047.
24. P. Hao, Y. Chen, T. Xiao, W.-H. Sun, *J. Organomet. Chem.*, 2010, **695**, 90–95.
25. (a) G. M. Sheldrick, *Acta Cryst*. 2015, **A71**, 3−8; (b) G. M. Sheldrick, *Acta Cryst.* 2015, **C71**, 3−8.

Journal Name

ARTICLE

GRAPHICAL ABSTRACT

Enhancing thermostability of iron ethylene polymerization catalysts through *N,N,N*-chelation of doubly fused α,α′-bis(arylimino)-2,3:5,6-bis(hexamethylene)pyridines

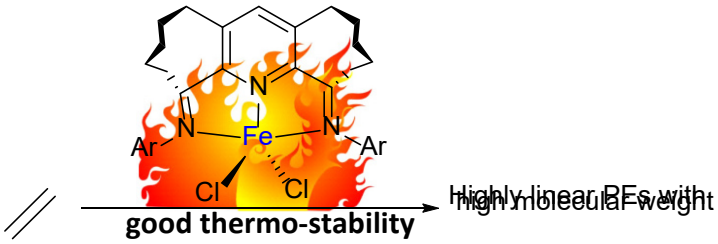

The α,α'-bis(arylimino)-2,3:5,6-bis(hexamethylene)pyridine-iron chloride chelates, **Fe1** – **Fe5**, on activation with either MAO or MMAO, possessed good thermo-stability and displayed high activities [up to 8.21 × 10^6 g(PE) mol^{-1} (Fe) h^{-1} at 80 °C] for ethylene polymerization affording strictly linear polyethylenes with high molecular weight.